ALTERNATIVE ALGORITHMS FOR HELICOPTER CONTROL SYSTEM BASED ON INVERSE DYNAMICS AND ITS UPGRADE WITH THE USE OF A SIDESTICK CONTROLLER

Aleksandr V. Efremov[1]   pvl@mai.ru
Eugene V. Efremov[1]   pvl@mai.ru
Zoe Mbikayi[1]   pvl@mai.ru
Sergei Yu. Esaulov[2]   sergey_esaulov@bk.ru
Valerii A. Ivchin [2]   vivchin@mi-helicopter.ru
Maksim I. Miasnikov[2]   mmyasnikov@mi-helicopter.ru

[1]Moscow Aviation Institute (RU), [2]Mil & Kamov National Helicopter Center (RU)

Abstract

The modern trend of developing highly automated aircraft is characterized by a transition from traditional methods and technical solutions to innovative approaches of creating control systems, inceptors, and displays. This paper deals with the development of helicopter control systems based on inverse dynamics and its integration with a novel type of side stick shaping the pilot output signal such that it is proportional to the control force (Force Sensing Control – FSC). The synergetic effect arising from this integration is also evaluated. The evaluation of the effectiveness of inverse dynamics was carried out through mathematical modeling of the pilot-aircraft system and ground-based simulations.

1. INTRODUCTION

The widespread implementation of automation means, characteristic of modern aviation, has been accompanied by research of new approaches to algorithm design.

The inverse dynamics technique is one of several techniques developed in the recent years that allow changing the dynamics of an aircraft considerably, making the control problem easier to solve.

It can be used as a nonlinear control technique based on feedback linearization or in the feedforward control loop. It has been used over the years for a variety of applications both in fixed-wing airplanes [1] and in rotorcraft [2].

The main issue when using inverse dynamics is the lack of robustness, as it requires exact mathematical models of the controlled element or of the processes affecting the controlled element, such as winds and disturbances. In [3] and [4], the author established the boundaries of controlled element uncertainties that would be acceptable when using inverse dynamics. The method developed in [3] allows using inverse dynamics only when these boundaries are observed. This makes the technique applicable only to a limited number of control problems.

As a nonlinear control technique, inverse dynamics is used to make an appropriate coordinate transformation of a nonlinear controlled element [5], so that any linear control technique can be applied to the resulting linear controlled element. This is illustrated in [2] and [6], where nonlinear dynamics inversion is used in the inner loop and a PID-type controller is used in the outer loop to achieve robustness against modeling uncertainties and disturbances. The same approach is used in [7], but robustness is provided by an H-infinity-based controller in the outer control loop.

As a linear control technique, inverse dynamics has mostly been used in the feedforward control loop to support feedback controllers. In this form, its integration with reference model techniques has been studied in [8]. Here, the desired dynamics of the whole system, that is, the controlled element plus the control system, are computed via the use of reference models. The computed desired dynamics are then given to the inverse dynamics in order to calculate the actuators positions needed to achieve the required performance.

This method, however, still requires an exact model of the controlled aircraft. Therefore, a PID-type compensator must be added in order to provide robustness against modeling uncertainties and disturbances as in [2].

Inverse dynamics as a linear control method has also been used in [9] to decouple the dynamics of the controlled element and achieve good tracking performance, and robustness is provided by a reference model and its inverse. This method, however, uses several loops in the control algorithm, making it difficult and expensive to implement.

In [10], a detailed account of the inverse dynamics

approach is given, where a PI controller is used to achieve the stability of the controlled element. The effectiveness of the proposed method is evaluated in the paper via pitch control task research using a flight simulator. The present paper briefly explains the approach proposed in [10], as well as studies its prospects in a hovering task with appropriate formulation of inverse dynamics.

This paper presents a method, in which a PI controller is used to provide robustness of the controlled element, and inverse dynamics are calculated in such a way that the inverse of the PI controller dynamics is taken into account. This approach allows it to effectively suppress the dynamics of the controlled element and the additional controller, therefore improving the tracking performances and decoupling the dynamics.

Different inceptors and types of pilot output signals were investigated with the goal of defining the best way of their integration with inverse dynamics.

2. MOTIVATION

The control systems algorithms are designed following the inverse dynamics method in a linearized helicopter mathematical model as shown in Figure 1.

Figure 1. Using inverse dynamics

Inverse dynamics are used in the feedforward loop to improve tracking performance, and require a stable system [11]. The stability is therefore provided by a set of feedback gains.

The use of inverse dynamics is motivated by the reasoning given in [10].

In Figure 1, $G^{-1}(s)$ is the inverse dynamics and $\dot{y}$ is the vector of angular rates and climb rate $[q, p, r, w]$.

The proposed algorithms bring the frequency response $\dfrac{\dot{y}(j\omega)}{\delta_c(j\omega)}$ closer to the gain response in a wide frequency range and decouple the control channels.

When the controlled element dynamics are $\dfrac{y(j\omega)}{\delta_c(j\omega)}$, the frequency response is then close to the integral element.

In Figure 1, the element **F(s)**, as shown in [10],

increases the order of the denominator, therefore making the system feasible, and the element

$$K_{1/s}(s) = K_s \frac{Ts+1}{s}$$

provides system robustness.

The frequency response of this process can be seen in Figure 2.

Figure 2. Inverse dynamics vs. feedback

3. CALCULATING INVERSE DYNAMICS

The inverse dynamics are calculated analytically, following the technique given in [11].

The system G contains nonlinear elements as shown in the previous section. Therefore it needs to be linearized and represented in the state space form before calculating the inverse dynamics. This is done using the Jacobian linearization method given in [12].

The obtained matrices A and B of the state space representation of the system G can be extracted by applying (8).

$$(8) \qquad \dot{\delta}_x(t) = A\delta_x(t) + B\delta_u(t)$$

Using the matrices A and B obtained above, the state space representation can be constructed as shown by (9) and (10).

$$(9) \qquad sX(s) = AX(s) + BU(s)$$

$$(10) \qquad Y(s) = CX(s)$$

where X is the state vector, U is the input vector and C is the matrix relating the state vector X to the output vector Y of the system G.

The transfer function representation can then be derived by re-writing (9) in terms of X(s) as shown in (11) and substituting it in (10) to obtain the equation (12):

$$(11) \quad X(s) = (sI - A)^{-1} \cdot BU(s)$$

$$(12) \quad Y(s) = C(sI - A)^{-1} \cdot BU(s)$$

The relationship between the state space representation and the transfer functions can then be written as:

$$(13) \quad \frac{Y(s)}{U(s)} = C(sI - A)^{-1} \cdot B$$

Equation 13 will result in a matrix of transfer functions, where each transfer function can be inverted individually such that for a transfer function $G(s) = \dfrac{y(s)}{u(s)}$ the inverse dynamics is given by $G^{-1}(s) = \dfrac{u(s)}{y(s)}$.

4. RESEARCH PLAN

The study considered two precision control tasks: pitch angle tracking and helicopter hover.

4.1. Plan of pitch angle tracking task research

This case includes a number of piloting tasks: acceleration and deceleration, slalom, and others. Here, pilot actions can be represented as a single-loop compensatory system shown in Figure 3.
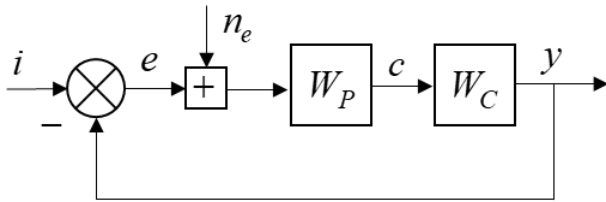
Figure 3. Pilot-aircraft system

The effectiveness of inverse dynamics in this task was studied using ground-based simulation and mathematical modeling of the pilot-aircraft system.

4.1.1. Mathematical modeling of the pilot-aircraft system

Mathematical modeling was carried out using a modified structural model of the pilot developed in [13] and shown in Figure 4.
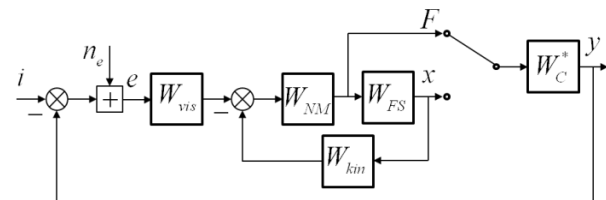
Figure 4. Modified pilot structural model

Here,

$W_{vis} = K_L \dfrac{T_L j\omega + 1}{T_I j\omega + 1} e^{-\tau j\omega}$ is the model of visual information perception and compensation;

$W_{kin} = \dfrac{K_n (j\omega)^2}{T_n^2 (j\omega)^2 + 2T_n (j\omega) + 1}$ is the model of proprioceptive information perception and compensation;

$W_{NM} = \dfrac{1}{(T_{N^*} j\omega + 1)} \dfrac{1}{(T_N^2 (j\omega)^2 + 2\zeta_N j\omega + 1)}$ is the neuromuscular system model;

$W_{FS} = \dfrac{K_{FS}}{(j\omega)^2 + 2\zeta_{FS}\omega_{FS} j\omega + \omega_{FS}^2}$ is the inceptor model;

n_e is the pilot noise (remnant), characterized by the spectral density $S_{n_e n_e} = K_{n_e} \pi \dfrac{\sigma_e^2 + T_L^2 \sigma_{\dot{e}}^2}{1 + T_L^2 \omega^2}$, where σ_e^2 and $\sigma_{\dot{e}}^2$ are the variances of error and its derivative, $K_{n_e} = 0.01$;

W_C^* is the controlled element dynamics which is the mathematical model of the vehicle and the flight control system dynamics. The parameter vector of the structural model $a = (T_L, K_L, T_n, K_n)$ is calculated by running the minimization criterion $I = \min \sigma_e^2$, where the variance of error σ_e^2 is determined by the equation given in [14].

The structural model shown in Figure 3 allows studying the pilot aircraft system for two types of pilot output signals. One of them is the displacement, performing the so-called "Displacement Sensing Control (DSC)", and the other is the force applied by the pilot, performing the so-called "Force Sensing Control (FSC)" [15].

4.1.2. Ground-based simulations

The effectiveness of inverse dynamics was also studied using a ground-based simulator equipped with a collimated visual system and the Moog control loading system (see Figure 5).

An image of the compensatory display was shown on the screen of the central collimator. The vertical motion of the indicator on this display allowed performing a compensatory pitch tracking task.

The Moog system equipped with force and displacement sensors allowed evaluating the effectiveness of the DSC and FSC types of pilot output.

The experiments involved two operators and one licensed pilot. They all had sufficient experience in ground-based simulations.

The compensatory pitch tracking task was carried out with a polyharmonic input signal

$$i(t) = \sum_{k=1}^{15} A_k \cos \omega_k t$$

, which appeared as a random signal to the operators. Its amplitude A_k and orthogonal frequencies $\omega_k = K \dfrac{2\pi}{T}$,where T is the duration of trials, were selected from the requirements of correspondence between the power distributions of the polyharmonic signal and a random signal characterized by the spectral density

$$S_{ii} = \frac{K^2}{(\omega^2 + 0.5^2)^2}, \sigma_i^2 = 4\,cm^2$$

.

The Fourier coefficient technique [16] was used for the calculation of the main pilot-vehicle system characteristics:

- Pilot $W_p(j\omega)$, open-loop $W_{OL}(j\omega)$ and closed-loop $\Phi(j\omega)$ describing functions.
- Pilot remnant spectral density $S_{n_e n_e}(\omega)$.
- Variance of error σ_e^2 and its components $\sigma_{e_i}^2$, which is the variance of error correlated with the input signal, and $\sigma_{e_n}^2$, which is the variance of error correlated with the remnant.

The experiments were carried out with the center and side sticks.

At least 3 trials were executed for each variable (controlled element dynamics, type of inceptor, and pilot output), and the identified results were averaged. The duration of each trial was equal to 144 s.

The following controlled element dynamics W_C^* were used in the experiments:

$W_C^* = W_{fb}$: dynamics of a controlled element whose control system consists of feedback only.

$W_C^* = W_{inv}$: dynamics of a controlled element whose control system includes feedback and inverse dynamics.

5. INVESTIGATION RESULTS

The results of the ground-based simulation, carried out for two types of flight control systems based on the use of traditional feedbacks only ($W_C^* = W_{fb}$) and inverse dynamics principle ($W_C^* = W_{inv}$), are shown in Figure 6.
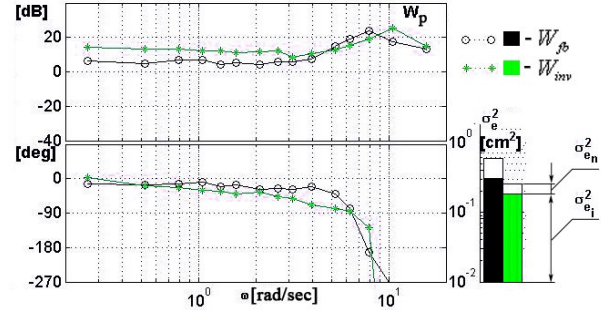
Figure 6. Results of experiments

It can be seen that when inverse dynamics is used, the variance of error σ_e^2 is 2.3 times less with a lower pilot lead phase compensation in the medium frequency range.

Qualitatively, close results were obtained in the mathematical modeling as well [10].

Both the pilot describing function and the frequency response of the closed loop system were calculated. This allowed calculating the parameters of the so-called "new MAI criterion for flying qualities prediction" [17].

The parameters of this criterion are the following:

- The bandwidth of the closed-loop system (ω_{BW}) corresponding to the frequency at which the phase response of the closed loop system is equal to -90 deg.
- The pilot compensation parameter ($\Delta\varphi_{max}$) calculated in the entire frequency range as the maximum difference between the pilot phase response of the investigated dynamics and that of the dynamics which do not require any pilot phase compensation (phase response corresponding to a time delay element).

The values of these parameters, calculated through mathematical modeling of the pilot-aircraft system in a hovering task and forward flight at a speed of V=230 km/h for two controlled element dynamics ($W_C^* = W_{fb}$, $W_C^* = W_{inv}$), are given in Figure 7.
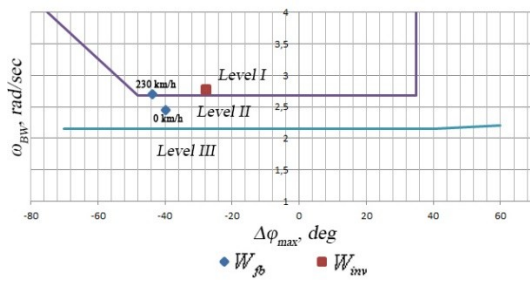
Figure 7. New MAI criterion

The results shown in Figure 7 demonstrate that the use of the inverse dynamics $W_C^* = W_{inv}$ in hover mode and at a speed of 230 km/h allows improving flying qualities, making them correspond to the 1st level.

In the case when the control system is based on feedbacks only, the flying qualities belong to the 2nd level.

The evaluation of the flying qualities using the Bandwidth / Time Delay criterion from ADS-33E-RPF for the same dynamics did not evidence that the all of the investigated dynamics belong to different levels.

A set of experiments were carried out to evaluate the effects of inverse dynamics with different types of inceptors (center and side sticks) on the pilot-aircraft system characteristics. The research demonstrated that for both the center and side sticks, the pilot lead compensation is lower for the DSC type of pilot output. As an example, Figure 8 demonstrates the pilot frequency response obtained for the side stick with both the DSC and FSC types of pilot output.
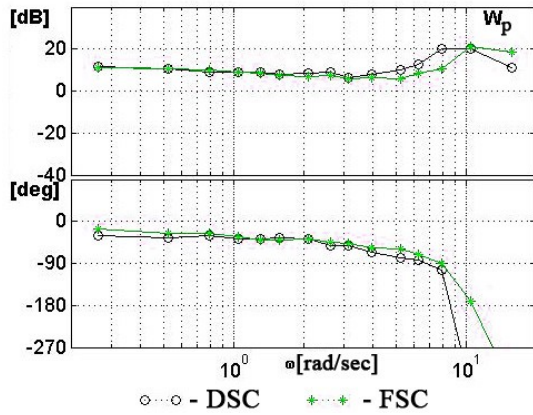
Figure 8. Pilot describing functions for DSC and FSC pilot outputs

In addition, the use of a side stick demonstrated a decrease in the variance of error σ_e^2 in the case where the DSC type of pilot output and traditional type of flight control system ($W_C^* = W_{fb}$) were used.

The variance of error σ_e^2 decreases by a factor of 1.1 to 1.3 (see Figures 9). The same consistencies were obtained in [13] for different aircraft dynamics configurations.

The experiments conducted for inverse dynamics with the same type of inceptor and pilot output demonstrated a decrease in the variance of error σ_e^2 by an additional factor of 1.8. When the FSC type of pilot output was used, the variance of error decreased even more, by a factor of 1.55. These results are shown in Figure 9.
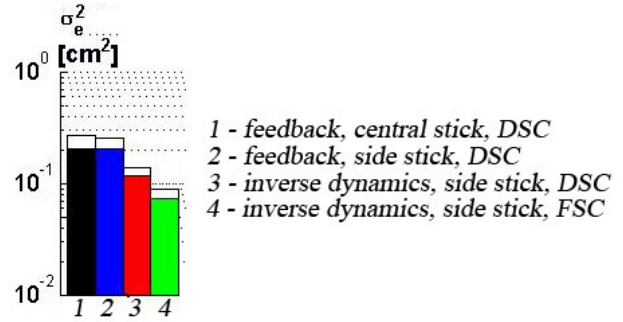

Figure 9. Variance of error

5.2 Plan of hovering task research

When performing a hovering task, the pilot aims to maintain the linear position of the rotorcraft *X(t)* relative to a set point on the ground. This task is characterized by the fact that in a rather large frequency range, the rotorcraft transfer function $\dfrac{X(p)}{æ(p)}$, where *æ(p)* is the cyclic pitch deflection, has the second pole order in the origin. It then follows, that performing this task requires that the pilot create additional control loops. A number of works [18, 19] consider the pitch angle to be such a loop. Alternatively, it is assumed in [20] that the pilot forms the inner loop after the sighting angle towards a certain object, located at a distance of

$$L = \sqrt{H_0^2 + X_0^2}$$

$$\varepsilon = \vartheta + arctg\,\frac{\Delta H}{\Delta X}$$

The linearization of this expression has the form of

$$\Delta \varepsilon = \Delta \vartheta + \frac{H_0}{X_0^2 + H_0^2}\Delta H$$

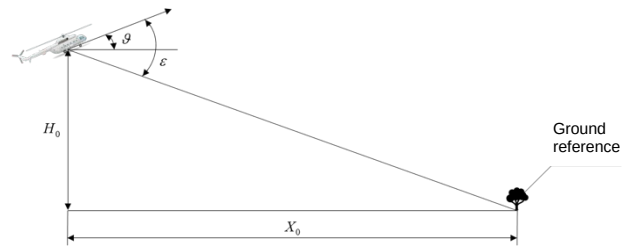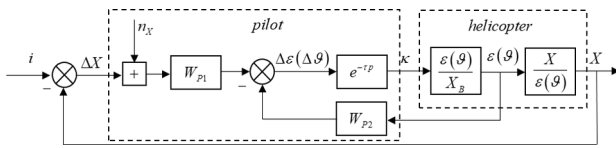The initial positions of the helicopter X_0, H_0 are shown in Figure 10.

Figure 10. Forming of sighting angle

Figure 11 shows a two-loop pilot-aircraft system in the hovering stage with alternative variants of inner loop forming by the pilot.

Figure 11. Pilot-aircraft system structure in hovering task

The present paper provides a comparison of two inner loop forming variants, as well as two variants of inverse dynamics in the inner loop: one of which provides closeness to the aircraft angular rate gain ω_z (the so-called RCAH control system case). This variant is hereinafter denoted as $ID\omega_z$. The other case provides the closeness of the frequency response $\dfrac{\vartheta(j\omega)}{\kappa(j\omega)}$ to the gain (the so-called ACAH control system case). It is hereinafter denoted as $ID\vartheta$. The pilot's choice of the optimal inner loop forming method (using the coordinate υ or ε) is largely determined by the frequency response relating the output coordinate $X(t)$ to the internal one. Frequency responses for both variants are given in Figure 12.
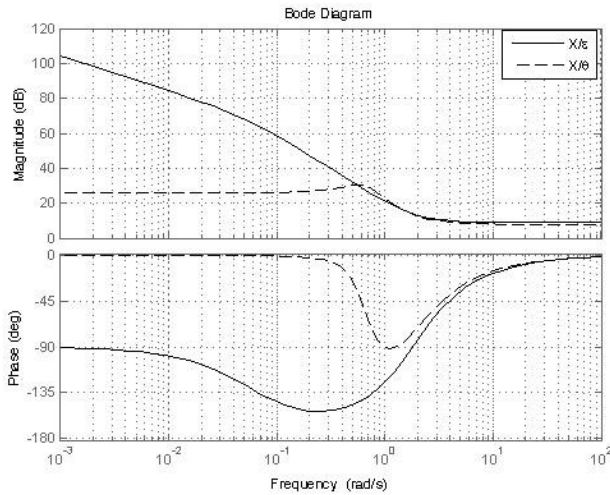

Figure 12. Bode plots of $\dfrac{X}{\varepsilon}$ and $\dfrac{X}{\vartheta}$

Their comparison shows that in the low and medium frequency area (ω=0.05 – 0.5 1/sec), that is, at frequencies characteristic of rotorcraft pitching motion, the slope of amplitude response $20\lg\left|\dfrac{X(j\omega)}{\varepsilon(j\omega)}\right|$ is close to 1, and the slope of amplitude response $20\lg\left|\dfrac{X(j\omega)}{\vartheta(j\omega)}\right|$ reaches -40 dB/dec. This allows us to assume that the forming of sighting angles by the pilot in the inner loop will provide high accuracy. The present study used a simplest visualization system in the form of a fixed line, denoting zero tracked coordinates, and two moving markers (see Figure 13).
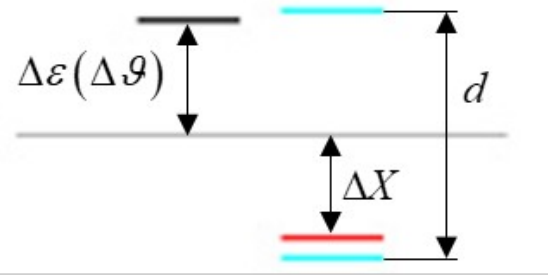
Figure 13. Visualization system

The experimental studies were carried out for two variants, wherein the distance to the center of the screen was proportional to the pitch angle $\upsilon(t)$ or the sighting angle ε. The distance between the right marker and the center of the screen was proportional to the error ΔX for both variants. Also displayed to the operator was the range d, which remained unchanged throughout the experiment and within which the pilot tried to keep the linear error. In addition to the variances of error and control stick deflection, the study also measured the equivalent pilot frequency response as the relation $\dfrac{\kappa(j\omega)}{e(j\omega)}$ of open-loop and closed-loop frequency responses. The study considered 3 variants of controller design:

– controller combining angle, angular velocity, vertical velocity, and altitude feedbacks;

– controller based on the inverse dynamics principle, providing RCAH response;

– controller based on the inverse dynamics principle, providing ACAH response.

The latter two cases also included feedback loops.

5.1. Hovering task study

The main pilot-aircraft system characteristics, obtained in experiments with different automation variants and loop-forming method, are given in Table 1.

Table 1. Primary pilot-aircraft system characteristics obtained through experimental research

Parameter	Inner loop ϑ			Inner loop ε		
	FB	$ID\omega_z$	$ID\vartheta$	FB	$ID\omega_z$	$ID\vartheta$
σ_e^2, cm^2	1.88	5.02	0.33	0.78	0.65	0.22
$\omega_c, rad/sec$	0.96	0.84	1.80	1.26	1.40	1.92
$\omega_{BW}, rad/sec$	1.03	0.94	3.82	1.76	1.49	4.70
r, dB	6.8	10.07	4.64	3.19	3.85	3.29
$\sigma_{\alpha_s}^2, deg^2/sec$	70.8	48.9	190.0	69.2	77.0	193.6

According to Table 1, the introduction of an additional loop by the pilot after the angle ε leads to a significant improvement in the primary characteristics of the pilot-aircraft system compared to the case introducing the inner loop after the angle ϑ for all considered automation variants. As such, for FB, the variance of error σ_e^2 decreases by a factor of 2.4, the crossover frequency ω_c increases by a factor of 1.3, the resonance peak r decreases by 3.6 dB, the bandwidth ω_{BW} increases by a factor of 1.6, and the variance of stick deflection σ_k^2 remains virtually unchanged.

For IDω_z, σ_e^2 decreases by a factor of 7.7, ω_c increases by a factor of 1.7, r decreases by a factor of 2.6, ω_{BW} increases by a factor of 1.6, and σ_κ^2 decreases by a factor of 1.5.

For IDϑ, σ_e^2 decreases by a factor of 1.5, ω_c increases by a factor of 1.1, ω_{BW} increases by a factor of 1.2, r decreases by 1.35 dB, and σ_k^2 remains virtually unchanged.

It should be noted that in the case of forming the inner loop after the angle ϑ, when switching from the automation variant FB to IDω_z, piloting accuracy in the first case decreases by 2.7 times. This is due to the fact that in the case of RCAH IDω_z controller, the pole order in the origin of the frequency response $\dfrac{X}{\kappa}$ in the frequency range between 0.01 rad/s and 1 rad/sec approaches $\dfrac{K}{p^3}$, which makes the piloting task more difficult in case of forming the inner loop after the pitch angle. Furthermore, in case of forming the inner loop after the angle ε, a similar switch from FB to IDω_z causes piloting accuracy to decreases by 1.2 times.

For the IDϑ automation variant, introducing the inner loop after the angle ε provides the highest piloting accuracy of all the considered variants (see Table 1) (compared to the case of introducing the inner loop after ϑ, the variance of error is 1.5 times lower), but leads to a significant variance of ω_z: 190 deg^2/sec^2 when forming the inner loop after the angle ϑ and 193.6 deg^2/sec^2 when forming the inner loop after the angle ε. In the rest of the considered variants, this value does not reach 80 deg^2/sec^2, and in the case of IDω_z when controlling the pitch angle, it does not reach 50 deg^2/sec^2. The highest variances of pitch angles are observed in FB and ID ω_z when controlling the angle ϑ (40.7 deg^2/sec^2 and 50.2 deg^2/sec^2 respectively). In other cases, σ_ϑ^2 are roughly comparable (≈ 33.75 deg^2).

We can therefore conclude that in a hovering task it is reasonable to use a control system based on the inverse pitch dynamics principle. In this context, the highest accuracy is achieved in case of forming the inner loop after the sighting angle. The influence of the resulting significant values of angular velocities on the piloting process requires further study using a flight simulator.

6. CONCLUSION

A control technique was developed by combining the inverse dynamics with the fight control system based on the use of feedbacks only.

The implementation of inverse dynamics and robustness requirements called for the installation of proper filters and PI controllers in the flight control system.

Experimental research has demonstrated the high effectiveness of inverse dynamics. Its integration with the side stick and the type of force sensing control at the pilot output allowed to reduce the variance of error in a pitch tracking task by 3 – 3.9 times compared to the traditional helicopter control system with feedback, the center stick, and DSC type of pilot output.

When performing a hovering task, it is expedient to study the inverse dynamics approach that provides ACAH response in conjunction with forming the inner loop after the pitch angle. This ensures the highest accuracy. The variance of error σ_e^2 reaches 0,22 cm^2, which is 8,6 times lower compared with attitude hold in control systems limited to feedbacks when forming the inner loop after the pitch angle.

7. REFERENCES

[1] Padhi R., Rao P. N., Goyal S. and Balakrishnan S. N. "Command tracking in high performance aircrafts: A new dynamic inversion design." IFAC Proc. 4 (7), 2007. doi:10.3182/20070625-5-FR-2916.00015

[2] Horn J. F. Non-Linear Dynamic Inversion Control Design for Rotorcraft. Journal Aerospace 6(3) 38, 2019. doi:10.3390/aerospace6030038

[3] S. Devasia. Robust inversion-based feedforward controllers for output tracking under plant uncertainty. Proc. of the 2000 American Control Conference, vol. 1, pp. 497-502, 2000. doi:10.1109/ACC.2000.878950

[4] S. Devasia. Should model-based inverse inputs be used as feedforward under plant uncertainty?. IEEE Trans. on Aut. Control, Vol.45, no. 11, pp. 1865-1871, 2002. doi:10.1109/TAC.2002.804478

[5] J. S. Brinker and K. A. Wise. Stability and flying qualities robustness of a dynamics inversion aircraft control law. Journal of Guidance, Control and Dynamics, Vol. 19, No. 6, November-December 1996. doi:10.2514/3.21782

[6] Ansari U. and Bajodah A. H. Robust generalized dynamic inversion based-control of autonomous underwater vehicles. Proc. of the Institution of

Mechanical Engineers, Part M: Journal of Engineering for the Maritime Environment 232(4) p434, 2018. doi:10.1177/1475090217708640

[7] Peng C., Han C., Zou J. and Zhang G. H-infinity Optimal Inversion Feedforward and Robust Feedback Based 2DOF Control Approach for High Speed-Precision Positioning Systems. Journal of Control Science and Engineering, Article ID 7256039, 2016. doi:10.1155/2016/7256039

[8] Miller C. J. Nonlinear Dynamic Inversion Baseline Control Law: Architecture and Performance Prediction. Proc. of the 2011 AIAA Conf. Guidance, Navigation and Control(Portland, OR, USA), 2011. doi:10.2514/6.2011-6467

[9] Z Mbikayi, A V Efremov and E V Efremov. Integration of the inverse dynamics with a reference model technique, and its application for the improvement of the helicopter flying qualities. IOP Conf. Ser.: Mater. Sci. Eng. 868 012016, 2020. doi:10.1088/1757-899X/868/1/012016

[10] Efremov A.V., Efremov E.V., Mbikayi Z., Esaulov S.Yu., Ivchin V.A., Myasnikov M.I. Synthesis of a helicopter control system using inverse dynamics and its upgrade with the use of a sidestick controller. 46th European Rotorcraft Forum, ERF 2020 Pages 9 - 172020 8 September 2020 - 11 September 2020

[11] Buchholz J. J. and Von Grunhagen W. Inversion Impossible?. Tech. Rep., Bremen university of Applied Sciences and DLR Braunschweig, Germany, 2008
 http://www.buchholz.hs-bremen.de/inversion/inversion_impossible.pdf

[12] Andrew Packard, Kameshwar Poolla, Roberto Horowitz. Dynamic Systems and Feedback. Class Notes for ME 132. Department of Mechanical Engineering, University of California. 2002. https://www.cds.caltech.edu/~murray/courses/cds101/fa02/caltech/pph.html

[13] A. V. Efremov, V. V. Aleksandrov, E. V. Efremov, M. V. Vukolov. The influence of different types of inceptors and their characteristics on pilot-aircraft system. 2nd IFAC Conference on Cyber-Physical & Human systems, Miami, Florida, USA, Dec. 2018. doi:10.1016/j.ifacol.2019.01.013

[14] Efremov A. V. Pilot-Aircraft system. Regularities and mathematical models of pilot behavior. pp. 1-193 MAI 2017.

[15] David H. Klyde and Duane McRuer. Smart-Cue and Smart-Gain concepts development to alleviate loss of control. Journal of Guidance, Control and Dynamics Vol. 32, No. 5, Sep-Oct 2009. doi:10.2514/1.43156

[16] Efremov A. V. et. al. Investigation of pilot induced oscillation tendency and prediction criteria development. WL-TR-96-3109 Wright laboratory pp. 1-138, USA May 1996.

[17] Efremov A. V., Efremov E. V. Tiaglik, M. S. Advancements in predictions of flying qualities, pilot-induced oscillation tendencies, and flight safety. Journal of Guidance, Control and Dynamics Vol. 43, No. 1, 2020. doi:10.2514/1.G004409

[18] Toader A., Ursu I. Pilot modeling based on time-delay synthesis. Proceedings of the Institution of Mechanical Engineers, Part G: Journal of Aerospace Engineering, vol. 228, 5: pp. 740-754., March 20, 2013.

[19] Hess, R. A. and Gorder, P. J. Design and evaluation of a cockpit display for hovering flight. Journal of Guidance, Control, and Dynamics, Vol. 13, No. 3, may 1990, pp. 450–457.

[20] A.V. Efremov, L.M. Anosova. Validation of the two-loop pilot-aircraft system structure. Thematic collection of studies "Manual control automation", Moscow, MAI 1989 (in Russian)